Cellular and Molecular Life Sciences
https://doi.org/10.1007/s00018-018-2928-3



ORIGINAL ARTICLE

# Deficiency of *lrp4* in zebrafish and human LRP4 mutation induce aberrant activation of Jagged–Notch signaling in fin and limb development

Jing Tian[1,6] · Jinhui Shao[1] · Cong Liu[1] · Hsin-Yu Hou[2] · Chih-Wei Chou[2] · Mohammad Shboul[3] · Guo-Qing Li[1] · Mohammad El-Khateeb[4] · Omar Q. Samarah[5] · Yao Kou[1] · Yu-Hsuan Chen[2] · Mei-Jen Chen[2] · Zhaojie Lyu[1] · Wei-Leng Chen[2] · Yu-Fu Chen[2] · Yong-Hua Sun[6] · Yi-Wen Liu[2]

Received: 11 April 2018 / Revised: 21 September 2018 / Accepted: 25 September 2018


## Abstract

Low-density lipoprotein receptor-related protein 4 (LRP4) is a multi-functional protein implicated in bone, kidney and neurological diseases including Cenani-Lenz syndactyly (CLS), sclerosteosis, osteoporosis, congenital myasthenic syndrome and myasthenia gravis. Why different *LRP4* mutation alleles cause distinct and even contrasting disease phenotypes remain unclear. Herein, we utilized the zebrafish model to search for pathways affected by a deficiency of LRP4. The *lrp4* knockdown in zebrafish embryos exhibits cyst formations at fin structures and the caudal vein plexus, malformed pectoral fins, defective bone formation and compromised kidney morphogenesis; which partially phenocopied the human *LRP4* mutations and were reminiscent of phenotypes resulting form a perturbed Notch signaling pathway. We discovered that the Lrp4-deficient zebrafish manifested increased Notch outputs in addition to enhanced Wnt signaling, with the expression of Notch ligand *jagged1b* being significantly elevated at the fin structures. To examine conservatism of signaling mechanisms, the effect of LRP4 missense mutations and siRNA knockdowns, including a novel missense mutation c.1117C > T (p.R373W) of *LRP4*, were tested in mammalian kidney and osteoblast cells. The results showed that LRP4 suppressed both Wnt/β-Catenin and Notch signaling pathways, and these activities were perturbed either by *LRP4* missense mutations or by a knockdown of LRP4. Our finding underscore that LRP4 is required for limiting Jagged–Notch signaling throughout the fin/limb and kidney development, whose perturbation representing a novel mechanism for LRP4-related diseases. Moreover, our study reveals an evolutionarily conserved relationship between LRP4 and Jagged–Notch signaling, which may shed light on how the Notch signaling is fine-tuned during fin/limb development.

**Keywords** Skeletogenesis · Bone disorders · Pronephros · Morphant · Phenocopy · EGF-like domain · *wt1b* · HES1

**Electronic supplementary material** The online version of this article (https://doi.org/10.1007/s00018-018-2928-3) contains supplementary material, which is available to authorized users.

✉ Jing Tian
tianjing@nwu.edu.cn

✉ Yi-Wen Liu
dlslys@thu.edu.tw

[1] The College of Life Sciences, Northwest University, #229 Taibai North Road, Xi'an 710069, China

[2] Department of Life Science, Tunghai University, No. 1727, Sec. 4, Taiwan Boulevard, Xitun District, Taichung 40704, Taiwan

[3] Department of Medical Laboratory Sciences, Jordan University of Science and Technology, Irbid, Jordan

[4] National Center for Diabetes, Endocrinology and Genetics, Amman, Jordan

[5] Orthopedic Division, Special Surgery Department, School of Medicine, The University of Jordan, Amman, Jordan

[6] State Key Laboratory of Freshwater Ecology and Biotechnology, Wuhan, China

Published online: 16 October 2018

## Introduction

The genes underlying the human genetic syndromes manifesting limb and digit malformations are well conserved in evolution, and some perform the same roles in the teleostean fins [1–3]. Using the zebrafish, the signaling pathways of fin development and regeneration can be well dissected. For example, the zebrafish has been developed as a model of Fraser Syndrome (FS), a recessive polygenic, multisystem congenital human disorder characterized by syndactyly of the soft tissue of digits, cryptophthalmos and renal agenesis. In the FS zebrafish mutant, the blister underneath the basement membrane of the fin epidermis is formed, which represents the limb malformation in FS patients [4]. The zebrafish model has also emerged as a powerful tool for dissecting molecular mechanisms that govern development, disease and regeneration of multiple organs or tissues such as the blood vasculature and the kidney [5, 6].

Low-density lipoprotein receptor-related protein 4 (LRP4) is a type I single transmembrane protein of the low-density lipoprotein receptor (LDLR) family. LRP4 mutations have been identified in Cenani-Lenz syndrome (CLS; MIM#212780) [7], congenital myasthenic syndrome 17 (CMS17; MIM 616304) [8] and Sclerosteosis 2 (MIM 614305) [9]. Different mutations in the *LRP4* locus result in distinct disease phenotypes: CLS is a rare autosomal recessive congenital disorder characterized by highly variable degree of syndactyly and/or oligodactyly of fingers and toes, which are associated with kidney agenesis or hypoplasia, nail aplasia or dysplasia, teeth anomalies and mild facial dysmorphisms; CMS17 patients present with neuromuscular disorder, but no syndactyly and kidney defects; Sclerosteosis 2 is a severe sclerosing bone dysplasia characterized by progressive skeletal overgrowth, with a variable manifestation of syndactyly. In contrast, the association between LRP4 and osteoporosis is revealed by genome-wide studies [10]. Autoantibodies against LRP4 has emerged as a diagnostic marker in Acetylcholine receptor (AChR)- and MuSK-negative myasthenia gravis [11]. The spectrum of disease phenotypes caused by various *LRP4* mutant alleles suggests a complicated role for LRP4 in development and homeostasis. Diverse functions of LRP4 have been further revealed by a series of mouse mutants, such as $Lrp4^{ECD/ECD}$, $Lrp4^{mte/mte}$, $Lrp4^{mitt/mitt}$ and $Lrp4^{mdig/mdig}$ [12–14]. The mutant mice present with syndactyly, characterized by the fusion and duplication of digits at both fore and hind limbs, some involve the malformation of carpal bones and entire limbs. Though renal anomalies are associated with some, but not all of the human *LRP4* mutations, they have been identified in the *Lrp4* mutant mice [15]. The *Lrp4* mutant mice also exhibit malformations of neuromuscular junctions, mammary glands and teeth. However, in patients with LRP4 mutation-associated bone diseases, no consistent neuromuscular dysfunctions have been described [16, 17]. Why different *LRP4* mutation alleles lead to distinct and even contrasting disease phenotypes is still unclear, and the answer may lie in the possible network of signaling pathways modulated by LRP4 protein.

LRP4 is localized exclusively to the plasma membrane of epithelial cells and demonstrates an antagonistic effect on LRP5/6-mediated activation of Wnt/β-catenin signaling, possibly due to a lack of an Axin-binding domain [12, 14]. However, the phenotypes of *Lrp4* mutant mice are more severe than what observed in *Lrp5* and *Lrp6* mutants [18, 19]. Moreover, novel ligands of LRP4 have been identified, including Wise, DKK1, Sclerostin, Gremlin1, Agrin, APP, MuSK, ApoE, Wnt9a and Wnt11 [16, 20–26]; which implicates multiple signaling mechanisms regulated by LRP4. The extracellular domain of LRP4 can interact with DKK1 and Sclerostin in osteoblasts, and with Wise in skin appendage and tooth development, suggesting that the Wnt inhibitory activity of LRP4 may depend on its interaction with the Wnt antagonists [22, 23, 26, 27]. However, LRP4 could also modulate Wnt/β-catenin signaling in tooth development through interacting with Wnt ligands in the absence of Wise [27]. LRP4 participates in the development of neuromuscular junction by interacting with Agrin, MuSK and APP [20, 21, 25]. In addition, LRP4 binds the BMP4 antagonist Gremlin1 in vitro [24], and is the receptor for ApoE in the rat brain [28]. These studies support the idea that LRP4 interacts with different ligands in a context-dependent manner. However, whether and how LRP4 serves to integrate multiple signaling pathways during dynamic processes of development and physiology remains to be investigated.

To explore how LRP4 regulates signaling pathways in different tissues, we have set out to identify and characterize the zebrafish ortholog of *lrp4*. A knockdown of zygotic RNA and protein expressions of the *lrp4* led to blistering of fin structures and caudal vein plexus, defective skeletogenesis and kidney phenotypes that partially phenocopied human LRP4 mutations, with an activation of Wnt/β-Catenin signaling pathway. Notably, we found that the Jagged–Notch signaling was activated in the fin structures upon a knockdown of *lrp4* in fish. In human embryonic kidney cells, LRP4 was confirmed to repress the Notch signaling activity, and this repressing activity was compromised by a novel missense mutation c.1117C > T (p.R373W) and other missense alleles of *Lrp4* that cause the CLS phenotype, a severe form of the *LRP4*-related diseases. Knockdown of *LRP4* expression in human osteoblasts induced upregulated expressions of Notch signaling components. Consistently, overexpression of *Lrp4* in mouse osteoblasts suppressed the expressions of Notch signaling components. The loss-of-function and overexpression results together implicate that abnormal activation of the Jagged–Notch pathway is a novel mechanism underlying the pathology of LRP4-related bone disorders. On the other hand, our study suggests that the negative regulation of Jagged–Notch pathway by LRP4 is a conserved mechanism shared between fin and limb development; possibly implicated in how Notch signaling controls the balance between self-renewal and differentiation.

## Materials and method

### Zebrafish husbandry

Zebrafish (*Danio rerio*) were raised according to standard protocols [29]. Embryos were obtained by natural crosses of wild-type and transgenic fish, and staged as previously described [30]. Embryos for histological analysis were treated with 0.03% phenylthiourea (Sigma) from 12-h post-fertilization (hpf) onwards to inhibit pigmentation. The following lines were used: *Tg(wt1b:GFP) (line1)* (from Christoph Englert, Fritz-Lipmann Institute, Jena, Germany); AB (ZIRC, Eugene, Oregon). All experimental procedures on zebrafish were approved by the Institutional Animal Care and Use Committee of Tunghai University (IRB Approval NO. 104-24) and carried out in accordance with the approved guidelines.

### Cloning of zebrafish *lrp4*

*lrp4* 5′RACE primers were designed and given in Table S1. 5′RACE was carried out using ExactSTART™ Eukaryotic mRNA 5′- & 3′-RACE Kit (Epicentre,USA). Twenty embryos at 6 hpf were collected and lysed by TRIzol Reagent (Ambion, USA). 10 µg total RNA was treated by alkaline phosphatase. The 5′ m7GPPPN structure of RNA was changed to 5′ single phosphoric acid by tobacco acid pyrophosphatase (TAP). 5′ adapters were ligated with 5′ single phosphoric acid RNA by T4 RNA ligase. First-strand cDNAs were synthesized by reverse transcriptase. After PCR amplification, target fragments were purified and TA cloned for screening. Full-length of *lrp4* was finally cloned to pCS2+ vector.

### In situ hybridization (ISH), immunohistochemistry (IHC), 3β-Hsd activity staining and Acridine Orange staining

Whole-mount ISH assays were performed as described in [31, 32] with modifications. Digoxigenin (DIG)-labeled riboprobes were synthesized from linearized plasmids containing *lrp4*, *fras1*, *pax2a*, *wnt5b*, *dkk1b* and *jag1b*, and DIG-labeled probes were detected with alkaline phosphatase conjugated anti-DIG antibody (Roche). The expressions were detected with BM purple (Roche). Stained embryos from the ISH assay were cleared in 50% glycerol in PBS, and photographed under Nomarski optics on an Olympus BX51 and Nikon SMZ25 microscope systems.

To detect the Lrp4 protein, *Tg(wt1b:GFP)* embryos were fixed and embedded in 4% NuSieve GTG low-melting agarose (Lonza), cut into 100 µm sections with a VT1000M vibratome (Leica), and permeabilized with PBS containing 1% Triton X-100 before incubation with mouse anti-LRP4 monoclonal antibody [S207-27] at 1:200 (Abcam). Dylight 650-conjugated anti-mouse IgG (Abcam) were used as secondary antibodies at 1:200. Images were captured with an LSM510 confocal microscope with version 3.5 software (Zeiss).

To quantify the distances between various tissue structures, images of embryos in each group were taken with identical magnification using an Axioskop 2 Plus microscope equipped with AxioVision 3.0 software (Carl Zeiss). Lengths were measured using Image Gauge Program, version 4.0 (Fuji Photo Film).

Histochemical staining for 3β-Hsd enzymatic activity was performed on whole embryos according to the described protocol [33]. For simultaneous analysis of interrenal steroidogenic activity and GFP fluorescence, 3β-Hsd staining signals were captured using transmitted light, while the fluorescent signals were captured with Argon 488-nm laser connected to the confocal microscope. Image processing and analysis was performed using the LSM 510 version 3.5 software.

Acridine orange staining to detect apoptotic cell death in living embryos was performed according to [34]. Live embryos at 2 days post-fertilization (dpf) were incubated in 2 µg/mL acridine orange (Sigma Aldrich) for 30 min followed by several rinses in the embryo medium, and were photographed using an LSM510 confocal microscope with version 3.5 software (Zeiss).

### Microinjection of morpholinos (MOs) and mRNA

MOs were synthesized at Genetools, LLC. The nucleotide sequences of the MOs were: *lrp4-sd* MO, 5′-ATC AGT GTT GTT GAT CTG ACC TGC A-3′; *lrp4-atg*MO, 5′-ACA AAG CAC CGC AGC GAG CCT CAT C-3′; *tp53*MO, 5′- GCG CCA TTG CTT TGC AAG AAT TG-3′ [35], STD-MO, 5′-CCT CTT ACC TCA GTT ACA ATT TAT A-3′ [36]. A 2 mM stock solution was prepared by dissolving lyophilized MO powder in 1 × Danieau solution before further dilution into the required concentrations. Full-length of mouse *Lrp4* cDNA was cloned into the pCS2+MT plasmid, and the capped mouse *Lrp4* mRNA was made by mMESSAGE mMACHINE SP6 Transcription kit (Thermo Fisher Scientific). MO- and mRNA-containing solutions were injected into one- to two-cell stage embryos using a Nanoject (Drummond Scientific). *tp53*MO, STD-MO and mouse *Lrp4* mRNA were injected at the dosage of 0.5 pmol, 1.2 pmol and 100 pg per embryo, respectively.

## Patients and clinical assessment

The patient was initially diagnosed at the National Center for Diabetes, Endocrinology and Genetics in Jordan. Genomic DNA from saliva samples from the four members of the kindred were obtained after parents gave their informed consent forms and the local ethics commission gave its approval. All human studies were approved by the Review Board of Northwest University.

## Mutation analysis

Direct candidate gene sequencing was performed. Primer pairs for each exon and the flanking intron regions of LRP4 were designed with Primer 3, and the primer sequences were given in Table S1. Sequence analysis was done with BigDye Terminator cycle sequencing kit and PCR products were run on ABI PRISM 3730 Analyzer (Applied Biosystems).

## Plasmids

Mouse *Lrp4* was subcloned into pcDNA3.1-3XFLAG from Lrp4-pcDNA3.1/V5-His-TOPO (kindly provided by Wollnik B. Laboratory). R373W, C160Y and D449N *Lrp4* mutant constructs were generated by site-directed mutagenesis. Mouse *Lrp6* was cloned into pcDNA3.1-3XFLAG. Mouse pUSE-Wnt1 was kindly provided by Virshup D. Laboratory. For construction of *Lrp4* overexpression stable lines, mouse *Lrp4* was subcloned into pCDH-CMV-MCS-EF1-Puro vector. pLP1, pLP2 and pLP-VSVG plasmids were purchase from System Biosciences (USA). Full-length zebrafish *lrp4* was cloned by RACE, and in-fusion to pCS2+vector. Zebrafish *fras1* plasmid was kindly provided by Carney TJ. Laboratory.

## Cell culture and transfections

HEK293T cells and MC3T3-E1 cells were maintained in DMEM (Gibco, USA) supplemented with 10% FBS (Gibco, USA), streptomycin and penicillin (Gibco, USA) at 37 °C. hFOB cells were obtained from ATCC (USA) and maintained in Ham's F12 DMEM (Gibco, USA) supplemented with 10% FBS (Gibco, USA) and 0.3 mg/ml G418 (Gibco, USA) at 33.5 °C. Cells were transfected with the use of Lipofectamine 3000 (Invitrogen, USA) according to the manufacturer's instructions.

## Luciferase assays

HEK293T cells were seeded at 700,000 cells/well in 6-well plates. To detect canonical Wnt signal pathway, transfections were performed in triplicate with the use of the TOP-Flash reporter system and the indicated expression plasmids with the following concentrations: 1000 ng wild-type (wt) *Lrp4* or 1000 ng mutants, 500 ng *Lrp6*, 500 ng *Wnt1*, 200 ng Topflash Vector, 10 ng Renilla (p-RL-TK). To detect Notch signaling pathway, transfections were performed in triplicate with the use of the HES1-pGL4.10 reporter system and the indicated expression plasmids with the following concentrations: 2000 ng wild-type (wt) *Lrp4* or 2000 ng mutants, 200 ng HES1-pGL4.10 Vector, 10 ng Renilla (p-RL-TK). Transfections were performed via Lipofectamine 3000 (Invitrogen, USA) according to the manufacturer's instructions. Two days after transfection, cells were lysed and luciferase activity was measured with the use of the Dual Luciferase Reporter Assay Kit (Promega, USA) and luminometer (Molecular Devices, USA). Each transfection was also measured in triplicates.

## RNA interference and stable line generation

hFOB cells were seeded at 700,000 cells/well in 6-well plates and transfected via Lipofectamine 3000 (Invitrogen,USA) with two siRNAs specific for human *LRP4* (100 pmol of each) or standard siRNA as a negative control. The siRNAs were purchased from GenePharma (China), and their sequences are given in Table S1. For SYBR green real-time PCR, cells were assayed 48 h after transfection. For stable line generation, HEK293T cells were seeded at 1000,000 cells per 100 mm dish, co-transfected with pLP1, pLP2, pLP-VSVG and pCDH-CMV-MCS-EF1-Puro-Lrp4-FLAG, after 72 h of transfection, the lentiviral particles were collected and concentrated. MC3T3-E1 cells were transfected with lentiviral particles, containing 5 μg/mL puromycin (Gibco, USA). Individual puromycin-resistant clone was isolated using separation rings, transferred, and sub-cultured.

## Reverse transcription PCR (RT-PCR) analysis

hFOB cells, MC3T3-E1 cells and zebrafish embryos were subject to total RNA extraction using TRIzol™ reagent (Ambion, USA). 1 μg of total RNA isolated from each sample was subject to cDNA synthesis by SuperScript™ system (Invitrogen). Semi-quantitative PCR was performed using Phusion Hot Start II DNA Polymerase (Thermo Fisher Scientific) and GeneAmp PCR System 2700 (Applied Biosystems), and ImageJ software was used for densitometric analysis. Quantitative PCR was performed with SYBR Green PCR Master Mix (Kapa Biosystems, USA) and ViiA 7 Real-Time PCR System (Applied Biosystems). The quantified values were generated from the average results of three independent experiments, and the value of each experiment was from the average of triplicate PCR runs. Primers sequences are given in Table S1.

### Statistical analysis

Each experiment was repeated at least three times, and the data were expressed as mean ± SE. The Student's *t* test was performed for comparing whether mean values were significantly different between two sample groups, whereas analysis of variance (ANOVA) followed by Duncan's new multiple range test (Duncan's multiple test) was used for multiple comparisons among mean values from more than two sample groups. $P < 0.05$ was considered statistically significant.

## Results

### Identification of the *lrp4* gene in the zebrafish

To investigate the LRP4 functions in vivo, we have isolated the complete cDNA sequence of *lrp4* in the zebrafish. Partial genomic and cDNA sequences of the zebrafish *lrp4* gene were obtained from Ensembl, and the full-length cDNA sequence was determined through a 5′-RACE method. Comparisons of the deduced amino acid sequence of the zebrafish Lrp4 to the human and mouse LRP4 sequences displayed a 77% overall amino acid identity (Fig. S1). Homology modeling of human, mouse and zebrafish proteins using SWISS-MODEL and PyMOL reveals that the structures of LDLa repeats, β-propeller domains, and EGF-like domains; where most of the known *LRP4* mutations are located, are all highly similar among the three species (Fig. S2). The high amino acid sequence homology and the conserved 3D structures lead to a hypothesis that the *lrp4* gene isolated from the zebrafish is a functional ortholog of the mammalian *LRP4*, and the biochemical properties of LRP4 are highly conserved among vertebrates.

ISH analysis revealed that the expression of *lrp4* mRNA was ubiquitous during stages of cleavage, gastrula and early somitogenesis (Fig. 1a), yet became restrictive from 24 hpf onwards (Fig. 1b). The *lrp4* mRNA was broadly expressed at the head region at 24 hpf, and was specifically distributed at the retina and the rhombic lips from 48 to 72 hpf. An evident expression of *lrp4* was detected at part of the dorsal spinal chord at 48 but not 72 hpf. At the pronephric kidney, the *lrp4* mRNA was clearly detected at 24 and 31 hpf and yet undetectable from 2 dpf onwards. As the zebrafish nephron is differentiated and functionally assembled at around 2 dpf, the results in Fig. 1b indicate that *lrp4* mRNA expression is activated at the kidney before the nephron differentiation. Meanwhile, the *lrp4* expression was abundant at pectoral fins from 31 hpf onwards. In the posterior trunk and tail regions, the *lrp4* gene showed a dynamic pattern of expression. The expression of *lrp4* at somites was strong at 24 hpf and weak during later stages. *lrp4* transcripts were detected at median fin fold at 24 hpf, at the posterior blood island (forming caudal vein plexus) at 31 hpf, and at the actinotrichia forming cells (AFC; essential for fin skeleton formation) from 48 to 72 hpf. The expression of *lrp4* in the developing zebrafish implicates its multiple roles for tissue formation and organogenesis, and is generally consistent with those in humans and in mice.

### Fin and kidney phenotypes in the zebrafish *lrp4* morphant

To model the disorders caused by a loss of LRP4 function, we performed *lrp4* MO injections in developing zebrafish embryos. The antisense MO was designed against the exon 15-intron 15 junction of the *lrp4* pre-mRNA. Injections of the *lrp4* splice-donor MO (*lrp4-sd*MO) into embryos specifically blocked the pre-mRNA splicing of the *lrp4* gene (Fig. S3A). Increasing dosages of *lrp4-sd*MO led to dose-dependent decrease in wild-type *lrp4* mRNA levels, as estimated by semi-quantitative RT-PCR analysis (Fig. S3b). On the other hand, quantitative RT-PCR (qRT-PCR) analysis using the intron-15 specific primer to detect expression levels of the mis-spliced product displayed an increase of mis-splicing from 0.2 to 0.4 pmol/embryo, yet essentially no significant difference among the dosage groups of 0.4, 0.6 and 1.2 pmol/embryo (Fig. S3C). In STD-MO but not *lrp4-sd*MO injected embryos, IHC analysis revealed the localization of Lrp4 protein in the retina, the inside of apical folds and the proximal region of the pectoral fin, as well as the kidney (Fig. 2a–f). Although a decrease of *lrp4* mRNA was evident in the *lrp4-sd* morphant as early as 10 hpf (Fig. S3a, b), no noticeable phenotype could be detected until 24 hpf. At 24 hpf, all of the *lrp4-sd* morphants displayed very mild dysmorphogenesis at the median fin fold and the caudal vein plexus (Fig. S4a). For the dosages higher than 0.2 pmol/embryo, the majority of *lrp4-sd* morphants displayed either single or multiple blisters at the median fin fold at 2 dpf. Therefore, we classified the *lrp4-sd* morphants into four categories according to the severity of median fin fold phenotypes (Fig. 2h). Moreover, the *lrp4-sd*MO caused a dose-dependent effect on the median fin fold, ranging from irregular edge to severe degeneration, which could be alleviated by a co-injection of mouse *Lrp4* mRNA (Fig. 2g, h). A co-injection of *tp53*MO did not rescue the blistering phenotypes (Fig. 2g), and no apoptotic cells were detected at the median fin fold of the *lrp4-sd* morphant (Fig. S4c), testifying that the blistering phenotype was not due to an

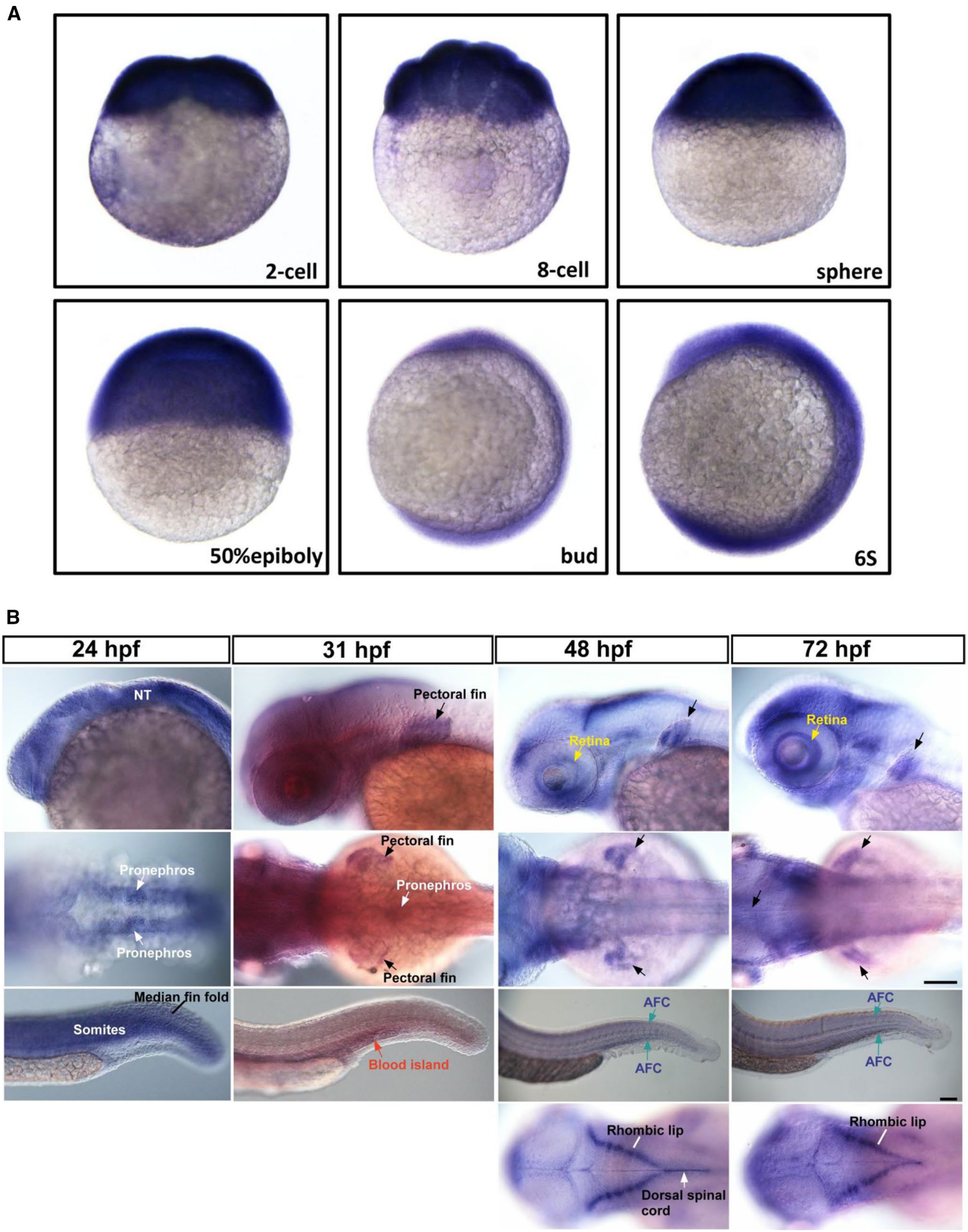
A
2-cell
8-cell
sphere
50%epiboly
bud
6S
B
24 hpf
31 hpf
48 hpf
72 hpf
NT
Pectoral fin
Retina
Retina
Pronephros
Pronephros
Pectoral fin
Pronephros
Pectoral fin
Median fin fold
Somites
Blood island
AFC
AFC
AFC
AFC
Rhombic lip
Dorsal spinal cord
Rhombic lip

◂**Fig. 1** The mRNA expression pattern of *lrp4* in the developing zebrafish**. a** The ubiquitous expression of *lrp4* mRNA during cleavage and gastrula stages. **b** The dynamic expression of *lrp4* mRNA at multiple tissues including the neural tube (NT) and the retina at the head (first row; lateral view with anterior towards the left); pectoral fins and pronephros at the midtrunk (second row; dorsal view with anterior towards the left); the median fin fold, somites, the (posterior) blood island, and actinotrichia forming cells (AFC) in the posterior trunk and tail regions (third row; lateral view with anterior towards the left). Restrictive expression of *lrp4* mRNA at rhombic lips and the dorsal spinal chord is evident from the dorsal view, starting from about 48 hpf onwards (last row). The ISH results shown are representative of at least 30 embryos for each stage

off-targeting effect mediated through p53 activation. An analysis of live *lrp4-sd* morphants revealed that the single blister phenotype (class II) was focused on the caudal vein plexus where the proliferation of hematopoietic stem cells occurs. Blisters in the class III embryos were distributed at both the caudal vein plexus and the posterior median fin fold (Fig. S4B). The results in Fig. 2g, S3b, S3c and S4b suggest that the dose-dependent effect of the *lrp4-sd*MO on posterior trunk and tail phenotypes are closely correlated with the extent of *lrp4* mRNA knockdown. In addition, all of the *lrp4-sd* morphants examined displayed dysmorphogenesis of the pectoral fin (Fig. 2i), and pectoral fin blistering were exhibited by class II-IV morphants.

To further verify the results of the *lrp4-sd*MO knockdown, an ATG morpholino (*lrp4-atg*MO) was utilized for phenotypic analysis. The results in Fig. S5a showed that the *lrp4-atg*MO caused essentially the same blistering phenotypes at the caudal vein plexus and the median fin fold, albeit with lower penetrance and expressivity.

To know whether a loss of *lrp4* function in the zebrafish affects the pronephric kidney development, we analyzed the kidney morphologies in *lrp4-sd* morphants which were classified into classes I to IV according to caudal fin phenotypes as described in Fig. 2h (Fig. 3a). *lrp4-sd*MO injections were performed on *Tg(wt1b:GFP)* embryos where developing kidney cells were marked by GFP, and the morphants were subjected to 3β-Hydroxysteroid dehydrogenase (3β-Hsd) activity staining for co-labeling steroidogenic interrenal tissues, the teleostean counterpart of the mammalian adrenal cortex. The kidney and interrenal morphologies were analyzed at 50 hpf when the pronephric nephron starts to function. The nephron morphology, as assessed by the distance from the lateral margin of proximal convoluted tubule to the midline, the length of pronephric neck segment, as well as the degree of convolution, was significantly compromised in all classes of *lrp4-sd* morphants (Fig. 3b, c). While kidney and interrenal cells were well segregated in all control embryos, the *wt1b:*GFP was detected in the steroidogenic interrenal tissues in 61.0% ($n=41$) of *lrp4-sd* class I morphants and 82.4% of class II morphants ($n=17$), indicating a defective segregation between kidney and steroidogenic interrenal cells (Fig. 3a).

Furthermore, the expressions of fin and kidney markers were significantly changed as detected by real-time qRT-PCR analysis in *lrp4* morphants (Fig. 4a, b). By 50 hpf, the expression of *fras1*, the zebrafish orthologue of the human Fraser syndrome gene *FRAS1* whose mutation leads to similar epidermal blistering, was increased in the median fin fold in *lrp4-sd* morphants as compared to control embryos (Fig. 4c, d). On the other hand, *pax2a* expression in pronephric duct and proctodeum was reduced in *lrp4-sd* morphants, which indicated a kidney malformation by loss of *lrp4* function in zebrafish (Fig. 4e, f). By 6 dpf, *lrp4-sd* morphants exhibited major skeletal anomalies by Alcian blue staining (Fig. 4g, h). Thus, the fin, kidney and skeletal phenotypes observed upon knockdown of *lrp4* in zebrafish partially phenocopy the human LRP4 mutations, revealing a conserved role of LRP4 in fin/limb development, kidney morphogenesis and skeletogenesis.

## Loss of Lrp4 function leads to upregulated Wnt and Notch signalings in the zebrafish

To check whether Lrp4 modulates Wnt/β-catenin signaling in the zebrafish, we analyzed the expression of Wnt/β-catenin pathway components by qRT-PCR (Fig. 5a). The expressions of many Wnt pathway components were increased in *lrp4-sd* morphants, remarkably labeled by Wnt receptor *fzd2*, co-receptor *lrp6*, ligand *wnt5b*, transcription factor *tcf7* and regulator *rspo1*. In contrast, the expression of Wnt inhibitor *dkk1b was* dramatically decreased. By 50 hpf, ISH analysis presented that the expression of *wnt5b* was increased in pectoral fin buds in *lrp4-sd* morphants (Fig. 5c). Meanwhile, *dkk1b* expression was visibly dampened in pectoral fin buds in *lrp4-sd* morphants compared to those of control embryos (Fig. 5d).

The loss of *lrp4* function in the zebrafish led to a kidney phenotype reminiscent of those resulted from defective Jagged–Notch signaling (Fig. 3a) [37]. A disruption of Jagged and Notch molecules has been shown to cause defective limb development in human and mice [38–40]. It is, therefore, of interest to examine whether the Jagged–Notch pathway is affected by a loss of *lrp4*. We discovered by ISH that the expression of *jag1b* demonstrates an evident and tissue-specific increase at the pectoral fin and the median fin fold (Fig. 5e, yellow arrows). Concomitant with the upregulated *jag1b* expression detected by ISH, qRT-PCR analysis of *lrp4-sd* morphants also exhibited significantly increased expression levels of Notch ligands *jag1b*, *jag2a* and *jag2b*; Notch receptor *notch2*; as well as Notch effectors *her1* and *her2*, indicating upregulated Notch signaling upon Lrp4 deficiency (Fig. 5b). In contrast, the expression of *lim1*, a target of Notch signaling whose expression is repressed by

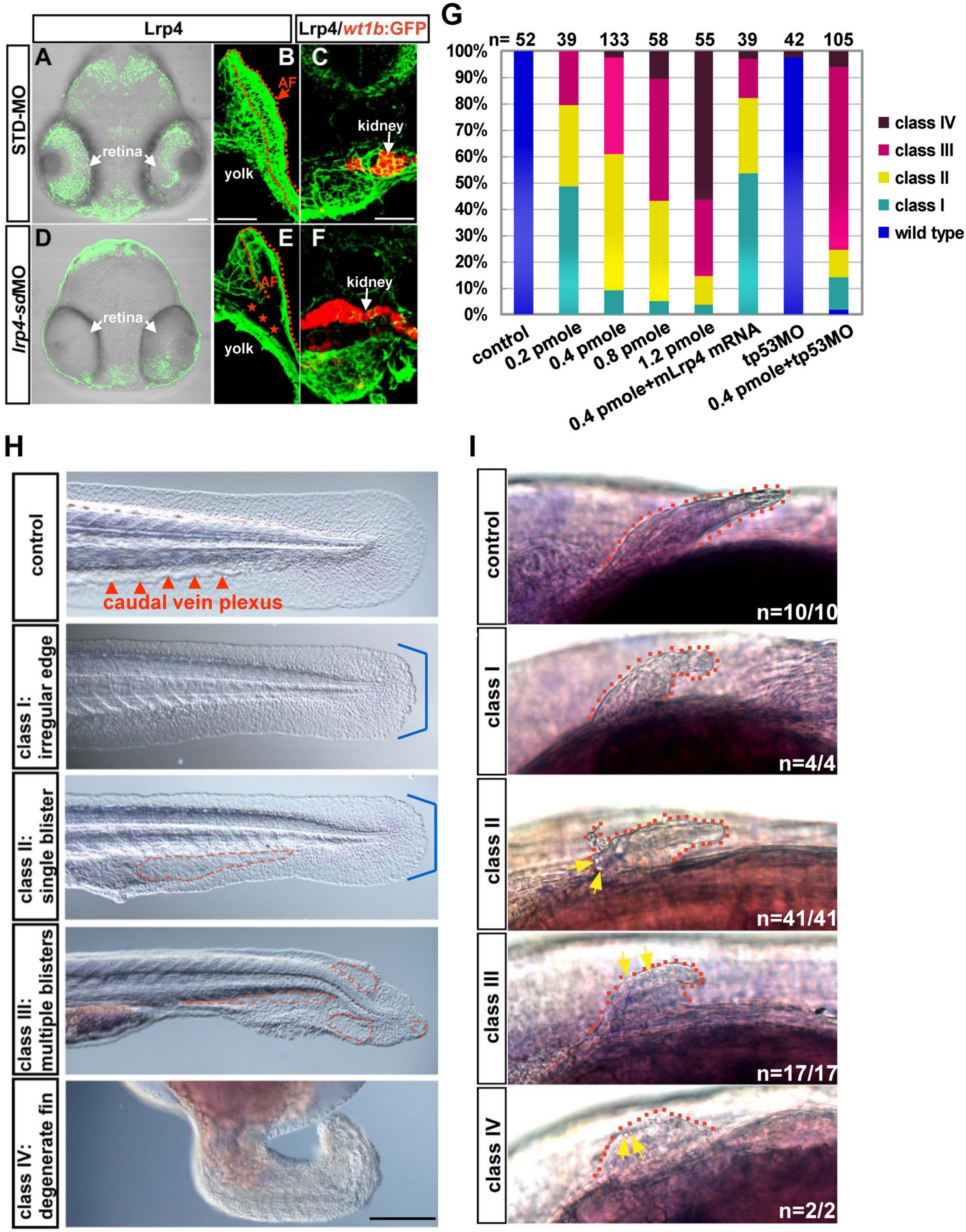

Lrp4
Lrp4/wt1b:GFP
A
B
C
D
E
F
G
H
I
STD-MO
lrp4-sdMO
retina
yolk
AF
kidney
n= 52
39
133
58
55
39
42
105
100%
90%
80%
70%
60%
50%
40%
30%
20%
10%
0%
control
0.2 pmole
0.4 pmole
0.8 pmole
1.2 pmole
0.4 pmole+mLrp4 mRNA
tp53MO
0.4 pmole+tp53MO
class IV
class III
class II
class I
wild type
control
caudal vein plexus
class I: irregular edge
class II: single blister
class III: multiple blisters
class IV: degenerate fin
control
n=10/10
class I
n=4/4
class II
n=41/41
class III
n=17/17
class IV
n=2/2

◂**Fig. 2** Phenotypes of the *lrp4-sd* morphant at the median fin fold and the pectoral fin. The expression of Lrp4 protein at the retina (**a**, **d**), pectoral fins (**b**, **e**) and the kidney (**c**, **f**) was compared between the STD-MO and *lrp4-sd*MO injected embryos. IHC analysis was performed on vibratome sections of 50 hpf *Tg(wt1b:GFP)* embryos injected with STD-MO (**a**–**c**) or *lrp4-sd*MO (0.4 pmol/embryo) (**d**–**e**) to detect the Lrp4 expression (green fluorescence; pseudo-color), while the *wt1b:*GFP was shown as red fluorescence (pseudo-color). The apical fold (AF) of the pectoral fin is highlighted by red broken lines. The absence of Lrp4 protein in the proximal region of the pectoral fin in the *lrp4-sd* morphant is indicated by red stars. The images of STD-MO and *lrp4-sd*MO injected embryos are representative of 4 samples for each treatment. **g** *lrp4-sd*MO led to a dose-dependent effect in the posterior trunk and tail regions, and the morphant phenotype was rescued by co-injected mouse *Lrp4* mRNA but not by *tp53*MO. **h** Classification of the *lrp4-sd* morphants is based on the phenotype of irregular fin edges (bracketed in blue) and formation of blisters (highlighted by broken red lines) as observed by Nomarski microscopy. **i** All classes of *lrp4-sd* morphants displayed small pectoral fins with irregular edges, and blisters (yellow arrows) were detected at the edge of pectoral fins of class II-IV morphants. Scale bar: 100 µm

the Notch pathway, demonstrated an evident decrease in the *lrp4-sd* morphant and further validated the activated Notch signaling. These results suggest that the Notch activity is negatively regulated by Lrp4 in the zebrafish. Expression levels of *jag1b*, *jag2a* and *her1* were also significantly elevated in the *lrp4-atg* morphant, however, with a less marked increase (Fig. S5B). The expression of *jag2b*, *notch2* and *her2* was activated by the *lrp4-sd*MO but not by the *lrp4-atg*MO, and the *limb1* expression was not suppressed by *lrp4-atg*MO. A comparison between the effects of *lrp4-sd*MO and *lr4-atg*MO implicates that the extent of Notch pathway activation may be correlated with the severity of *lrp4* knockdown phenotype.

### A novel missense mutation in the 1st EGF-like domain of LRP4 represses canonical Wnt signaling activity

While the Jagged–Notch signaling pathway was found to be antagonized by Lrp4 in the zebrafish, we sought to investigate whether the mechanism is relevant to the human *LRP4* mutation. The patient from a consanguineous Jordanian family was examined and presented with a typical expression of CLS clinical symptoms, mainly including short forearms, radius-ulnar synostosis, syndactyly of hands and feet, disorganized metacarpal and phalangeal bones, nail aplasia, as well as vertebral anomalies. The lower extremities were less severely affected than upper limbs (Fig. 6a–c′). Renal agenesis, presenting with absence of right kidney and hypertrophy of left kidney, was also observed (Data not shown). The index patient was subjected to Sanger sequencing of *LRP4*, and a novel missense mutation c.1117C > T (p.R373W) was detected. This variant was observed in a homozygous state in the index patient while heterozygous in her parents and the unaffected sibling (Fig. 6d). The variant was not found after being further screened in at least 100 healthy control individuals. This missense mutation is located in the 1st extracellular EGF-like domain of LRP4 (Fig. 6e), highly conserved across various species (Fig. 6f).

To examine whether the R373W mutation leads to loss of LRP4 function, we performed TOP-Flash luciferase assay to analyze the effect of R373W mutation on the activation of canonical Wnt signaling. Similar to C160Y and D449N missense mutations [16], R373W abolished the antagonistic LRP4 effect on LRP6-mediated activation of Wnt/β-catenin signaling (Fig. 6g), which could be due to the failure of mutant LRP4 to be efficiently transported to the plasma membrane. The effect of R373W missense mutation, along with the siRNA knockdown, was then utilized for studying how loss of LRP4 function affects Jagged–Notch signaling.

### Jagged–Notch signaling is activated by loss of LRP4 function and repressed by LRP4 overexpression

To investigate whether the Notch activity was negatively regulated by the LRP4-mediated signaling in mammalian cells, we examined how wild-type and mutant forms of mouse *Lrp4* affected the Notch pathway by a dual luciferase reporter assay in HEK293T cells. We found that *Lrp4* was able to antagonize the Notch activation. In contrast, coexpression of *Lrp4* C160Y or R373W mutant with the reporter of Notch effector Hes1 abolished the antagonistic effect of *Lrp4* on Notch signaling (Fig. 7a). Analysis of siRNA knockdown of human *LRP4* in hFOB cells exhibited markedly increased NOTCH signaling by the expression of *NOTCH1*, *NOTCH2* and *HES1* (Fig. 7b). Consistent with the upregulation of Notch signaling by *LRP4* knockdown in hFOB cells, the expression of Notch signaling pathway components was significantly reduced in mouse *Lrp4*-overexpressing stable MC3T3-E1 cells (Fig. 7c). Taken together, our results from zebrafish, human and mouse cells show that both Wnt/β-catenin and Notch pathways were activated upon the LRP4 deficiency, suggesting a cross talk between the two pathways.

## Discussion

The analysis of sequence, expression and phenotype of the zebrafish *lrp4* gene in this study supports that the structure and function of LRP4 are conserved between fish and mammals. The knockdown of *lrp4* mRNA in the *lrp4-sd* morphant (Fig. S3A,B) resembles the severe yet incomplete reduction of *Lrp4* mRNA in the $Lrp4^{dan/dan}$ mouse mutant [13]. However, $Lrp4^{dan/dan}$ exhibits syndactyly but no noticeable kidney agenesis. The major mis-spliced product in the *lrp4-sd* morphant (Fig. S3a, c), if successfully

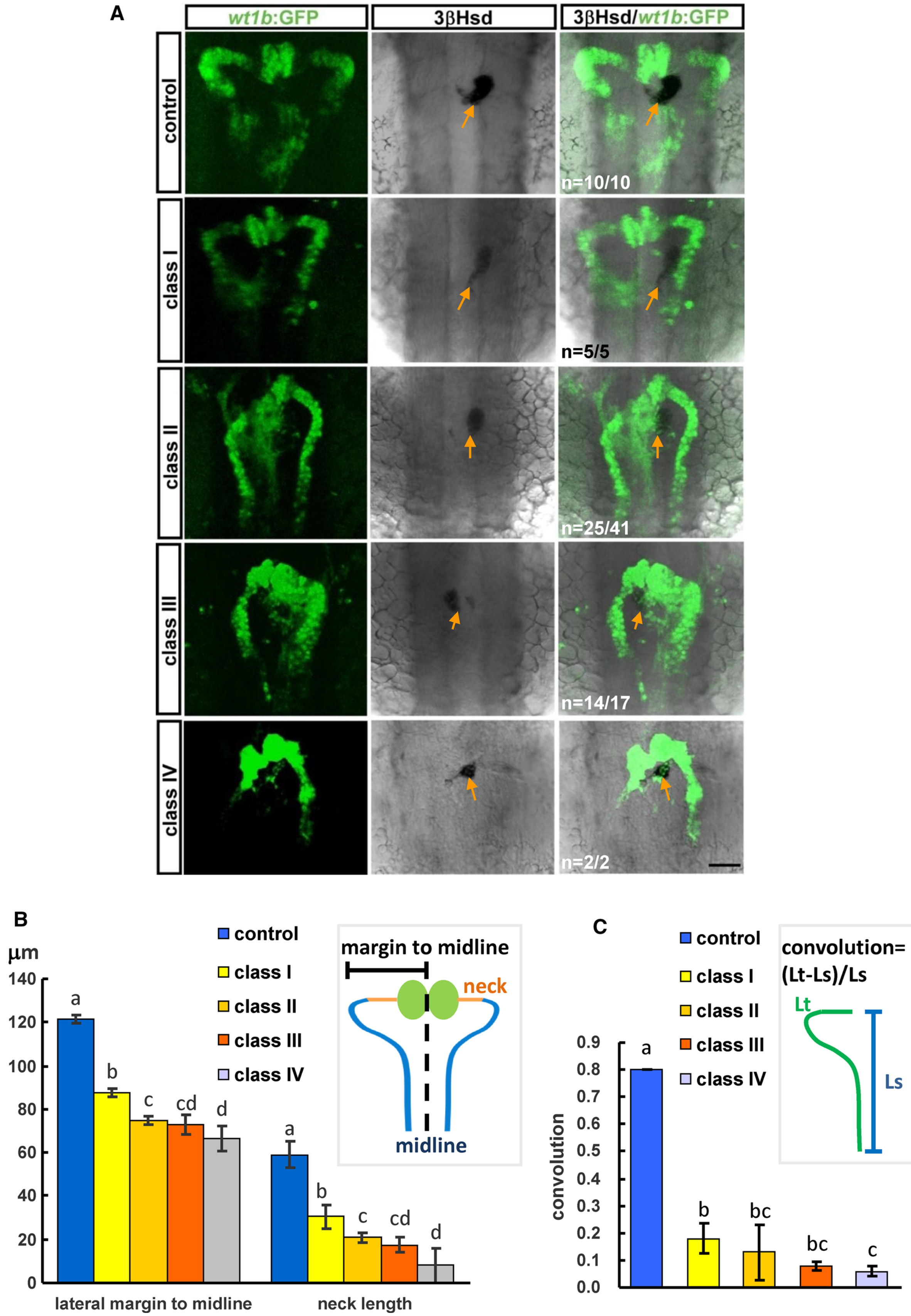
A
wt1b:GFP
3βHsd
3βHsd/wt1b:GFP
control
class I
class II
class III
class IV
n=10/10
n=5/5
n=25/41
n=14/17
n=2/2
B
μm
control
class I
class II
class III
class IV
margin to midline
neck
midline
lateral margin to midline
neck length
C
convolution=
(Lt-Ls)/Ls
Lt
Ls
convolution

◂**Fig. 3** The phenotype of kidney and interrenal tissue in the *lrp4-sd* morphant. **a** The kidney morphology was delineated by the *wt1b:*GFP, and the steroidogenic interrenal cells were detected by 3β-Hsd activity staining (orange arrows). **b** The pronephric structure was quantified by measuring the average distance from bilateral margins to the midline, and the average length of bilateral pronephric necks. **c** The pronephric convolution was arbitrarily defined as the ratio of the length of the proximal pronephric tubules marked by the *wt1b:*GFP (Lt) minus the length of a straight line connecting the ends of this segment (Ls) divided by the length of this straight line. Histograms with different letters above them are significantly different (ANOVA and Duncan's multiple test, $P<0.05$)

translated, is expected to result in one substitution at the end of 1st β-propeller domain (G701Q) followed by 26 incorrect amino acids, leading to a premature stop codon. It cannot be ruled out that the putative truncated protein resulted from the mis-spliced product may also play a role for the *lrp4-sd* morphant phenotype. The mouse *Lrp4 mitt* allele that contains an early stop mutation at the 1st EGF-like domain (Q377 stop) demonstrates phenotypes including syndactyly, kidney agenesis and early death [14]; which are more severe than those caused by the *Lrp4 dan* allele. In human, a homozygous nonsense mutation at the very beginning of the large extracellular domain (p.E97X) leads to severe CLS phenotypes including renal hypoplasia/agenesis [41]. Compound heterozygosity of a nonsense allele (p.K801X) and a frameshift allele (p.S1020Qfs*27) results in a prenatal lethal form of CLS [42]. These studies support that the truncating mutations of LRP4 cause more severe phenotypes. It is possible that the fin and kidney phenotypes in the *lrp4-sd* morphant are resulted from combinatorial effects of *lrp4* mRNA reduction and mis-spliced RNA product, although the effect of the mis-spliced RNA product may not be MO dose-dependent (Fig. 3c). Characterization of the *lrp4* gene in the zebrafish led us to discover that *lrp4* acted as an antagonist of Jagged–Notch signaling during development. This finding in fish has further been confirmed by the studies of human missense *LRP4* mutations, knockdown of *LRP4* by siRNAs, and overexpression of *Lrp4*. The Notch activity, quantified by the HES1 reporter assay in embryonic kidney cells, was repressed by LRP4, and the repressing effect was partially abrogated by R373W and C160Y mutations. Through siRNA knockdown and lentivirus-mediated stable expression of Lrp4 in osteoblasts, both Wnt/β-Catenin and Jagged–Notch signaling pathways were found to be activated by a deficiency of *LRP4* and suppressed upon the overexpression of *Lrp4*. The experiments in human and mouse

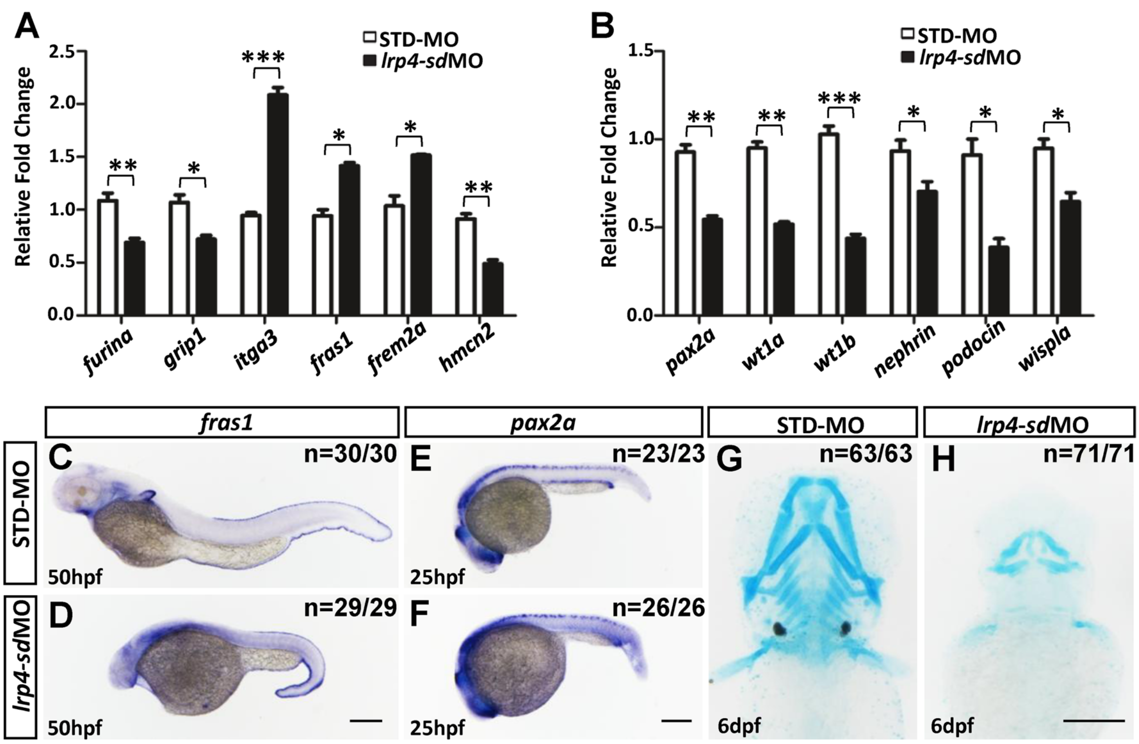


**Fig. 4** *lrp4* knockdown in zebrafish embryos affects gene expressions in the skeletal and kidney development. The expressions of fin (**a**) and kidney (**b**) markers, as determined by qRT-PCR, were significantly changed in *lrp4-sd* morphants at 2 dpf. The results of qRT-PCR were the average of triplicate experiments using 10 embryos in each treatment group for one RT reaction. **c** STD-MO injected control and **d** *lrp4-sd* morphant embryos at 50 hpf stained for the fin marker *fras1*. Note the enhanced expression in the median fin fold of *lrp4-sd* morphants. **e** STD-MO injected control and **f** *lrp4-sd* morphant embryos at 25 hpf stained for the kidney marker *pax2a*. Note the reduced expression in the pronephric duct and the proctodeum of *lrp4-sd* morphants. Alcian blue staining showed severe skeletal anomalies in *lrp4-sd* morphants (**h**) compared with STD-MO-injected control (**g**) embryos at 6 dpf. Scale bar: 200 µm. Values in **a** and **b** represent mean ± SE of data from three independent experiments, $*P<0.05$, $**P<0.01$, and $***P<0.0001$ (Student's *t* test)

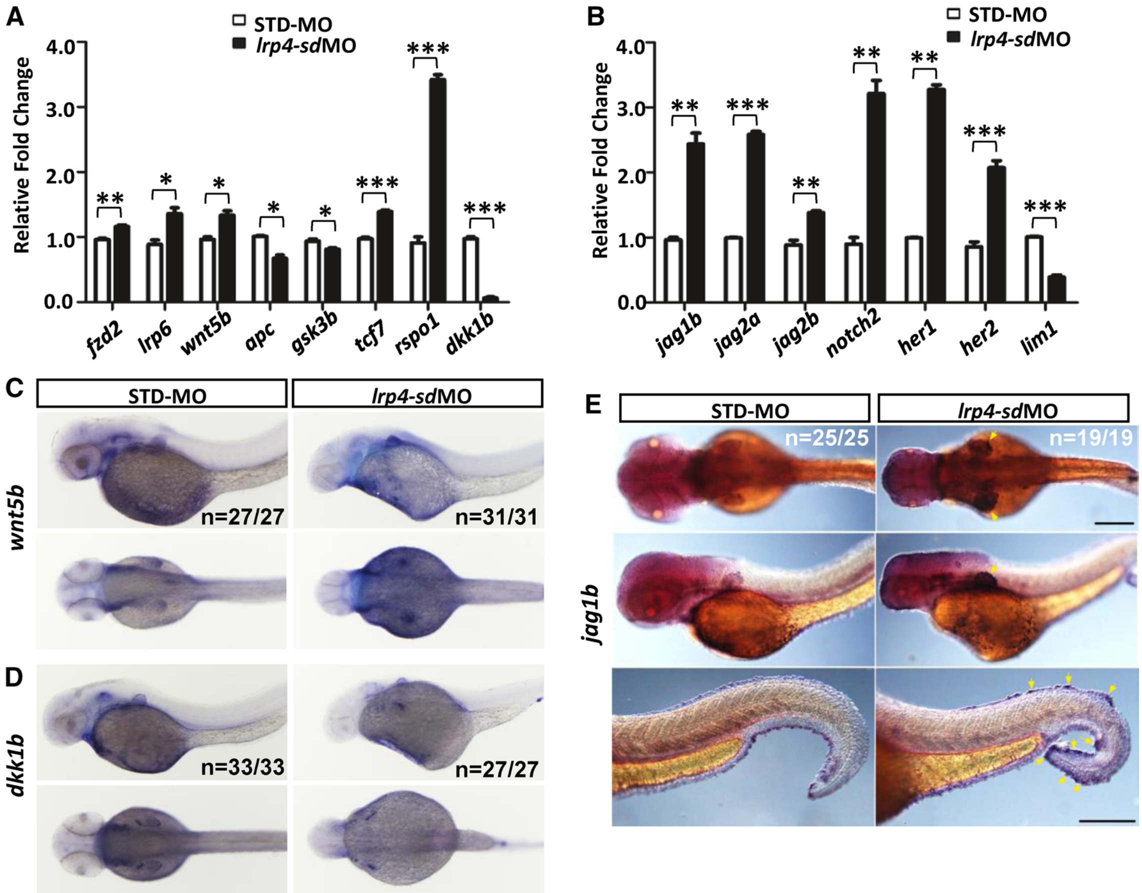


**Fig. 5** The activation of Wnt and Notch pathways in *lrp4-sd* morphants. The expression of genes which are components of Wnt pathway (**a**) or Notch pathway (**b**) was quantitatively analyzed by qRT-PCR for *lrp4* morphants (black bar) and STD-MO injected control embryos (white bar) at 2 dpf. The results of qRT-PCR were the average of triplicate experiments using 10 embryos in each treatment group for one RT reaction. ISH analysis of *wnt5b* (**c**), *dkk1b* (**d**) and *jag1b* (**e**) expressions was performed on the *lrp4-sd* morphant and STD-MO injected control embryos. Scale bar: 200 μm. Values in **a** and **b** represent mean ± SE of data from three independent experiments, $*P<0.05$, $**P<0.01$, and $***P<0.0001$ (Student's *t* test)

osteoblast cells, as well as those in human embryonic kidney cells, therefore, testified the inhibitory action of *LRP4* upon Jagged–Notch signaling activity in mammals.

While this study suggests that LRP4 is required for negatively regulating the Jagged–Notch pathway, it is intriguing to ask the biological importance of this mechanism during fin/limb development. In mammalian osteoblastogenesis and chondrogenesis, the Notch signaling activity serves to maintain stemness of progenitors by inhibiting osteoblast or chondrogenic cell proliferation [40, 43]. Consistently, in the regenerating adult zebrafish fins, the Notch signaling activity promotes proliferation of undifferentiated precursor cells in the blastema and prevents osteoblast differentiation. Therefore, in the skeletal development of mammals and fish, the Notch signaling activity is critical for maintaining a balance between self-renewal and differentiation. In this regard, the function of LRP4 may serve to ensure osteoblast differentiation in the developing fins/limbs. Interestingly, the upregulation of Jagged–Notch signaling in the *lrp4-sd* morphant is reminiscent of the knockdown phenotype of *chsy1*, a zebrafish orthologue of human Temtamy preaxial brachydactyly syndrome (MIM 605282) [3], implicating that aberrantly upregulated Jagged–Notch signaling is an important pathogenic mechanism for limb/fin morphogenetic disorders.

It is possible that different mutation alleles of LRP4 exert differential effects on the balance of Jagged–Notch signaling, thus leading to distinct bone phenotypes including syndactyly, sclerosteosis, and osteoporosis. Syndactyly, sclerosteosis and osteoposis are all known to be associated with dysregulations of Notch signaling whose strength and activity levels are critical for skeletal development and bone remodeling. For example, Notch gain of function in the osteoblasts of transgenic mice leads to increased number of osteoblasts and massive sclerosteosis [44]. Osteoporosis is manifested in Hajdu-Cheney Syndrome due to a sustained activation of

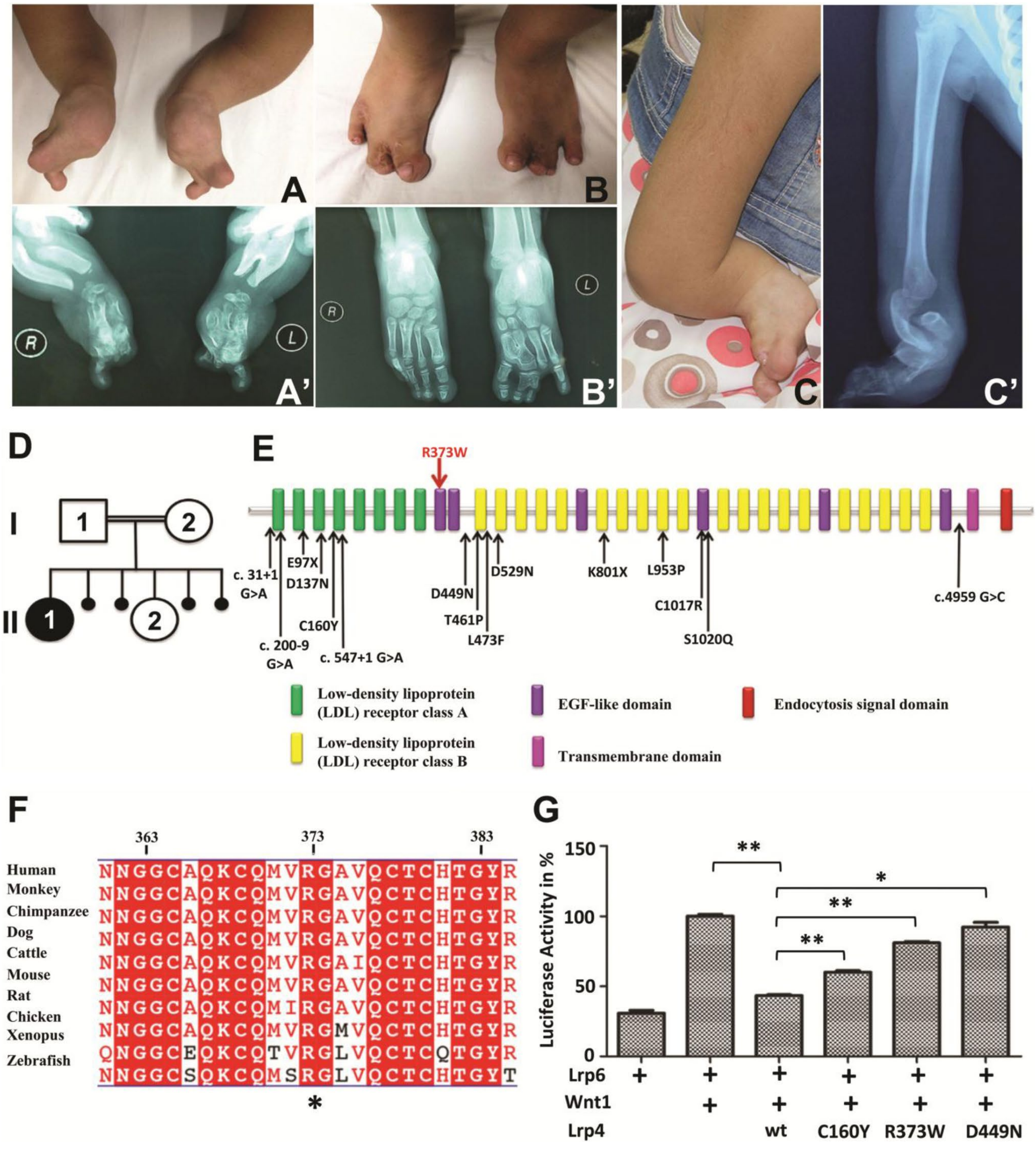


**Fig. 6** Phenotypic characteristics of investigated patient with typical Cenani-Lenz syndactyly syndrome caused by a point mutation in *LRP4*. The picture (**a**) and X-ray radiograph (**a′**) of patient's hands, the picture (**b**) and X-ray radiograph (**b′**) of patient's feet, showing syndactyly, disorganized metacarpal and phalangeal bones. The picture (**c**) and X-ray radiograph (**c′**) of patient's right upper limb, showing short forearms and radius-ulnar synostosis. **d** The patient, female (II:1), was born to first cousin parents (I:1 and I:2) with one unaffected child (II:2) and four abortions. **e** Schematic view of LRP4 domains and localization of identified CLS mutations, where the novel mutation R373W is labeled by the red arrow and other known mutations labeled by black arrows. **f** LRP4 is highly conserved across different vertebrate species; the conserved R373 is highlighted with a star (*). **g** The effect of R373W mutation and *LRP4* knockdown on the Wnt signaling in vitro. TOP-Flash luciferase assay was performed to quantify the Wnt activity in HEK293T cells co-transfected with *Lrp6*, *Wnt1*, and the indicated *Lrp4* cDNA. Values represent mean ± SE of data from three independent experiments, $^{*}P<0.05$, $^{**}P<0.01$. (Student's *t* test)

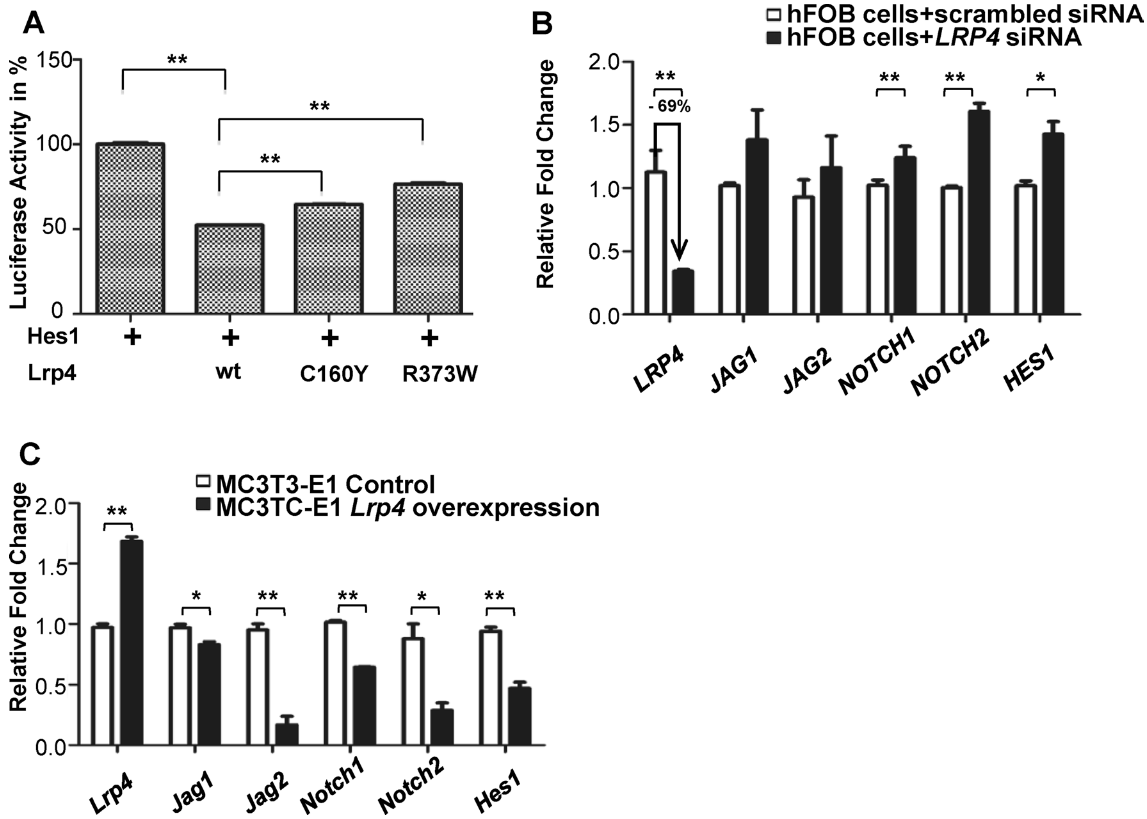


**Fig. 7** Loss of LRP4 results in activation of Notch signaling. **a** Dual luciferase reporter assay to quantify the Notch signaling activity as Hes1 was coexpressed with the indicated *Lrp4* cDNA in HEK293T cells. **b** *LRP4* siRNA in hFOB cells achieved 69% knockdown with upregulated gene expressions of NOTCH signaling components. **c** Gene expressions of Notch signaling components were downregulated when *Lrp4* was overexpressed stably in MC3T3-E1 cells. Values in **a**–**c** represent mean ± SE of data from three independent experiments, *$P < 0.05$, **$P < 0.01$. (Student's *t* test)

NOTCH2 activity [45], and *JAG1* polymorphisms are correlated with risk of osteoporotic fracture in several populations [46]. Mutations of *Jag2* cause syndactyly in mice [39]. It remains unknown how and through which domain LRP4 modulates the Jagged–Notch activity, and whether relative abundance of Notch pathway components in various tissues could partially account for the distinct phenotypes caused by *LRP4* mutations. As the expression of *Jag1b* was significantly increased in the zebrafish *lrp4-sd* morphant (Fig. 5e), it is possible that the Jagged–Notch signaling may function downstream of the canonical Wnt pathway in the zebrafish embryo. However, it may not be ruled out that the Notch pathway and Canonical Wnt pathways could also be modulated in a parallel manner, either directly or indirectly, by LRP4. It will be of interest to explore whether different *LRP4* alleles, that cause distinct disease phenotypes and implicated in different pathways, would differentially affect the gene expression and function of the Jagged–Notch pathway.

We also provide evidence to support that abnormally increased activity of the Jagged–Notch signaling may, at least partially, explain the often association between limb and kidney disorders in the human *LRP4* mutation. Upregulated expressions of Jagged–Notch signaling pathway components in either kidney podocytes or tubules have been implicated in diabetic nephropathy, folic acid-induced kidney injury and focal segmental glomerulosclerosis [47, 48]. While *Jagged2* (*Serrate2*) mutant mice exhibit syndactylism due to defects in limb-bud patterning and interdigital apoptosis [38, 39], knockdown of either *jagged2* or *notch3* in the zebrafish disrupts development of the pronephric duct [49, 50]. These reports and our study together point out that precise control of Jagged–Notch signaling is essential to prevent limb defects and kidney anomalies.

The dysmorphogenesis of fin and caudal vein plexus in the *lrp4* zebrafish morphant highly resembles that in the reported zebrafish mutations of human Fraser syndrome (MIM 219000) [4], indicating a link between *lrp4* and Fraser syndrome genes for the extracellular matrix patterning. Mutations of large basement membrane protein-encoding genes including *FRAS1* (MIM 607830), *FREM1* (MIM 608944) or *FREM2* (MIM 608945) lead to the Fraser syndrome in humans, and a blebbed phenotype in mice; both are characterized by syndactyly and bilateral renal agenesis

[51, 52]. Mutations of Fraser genes in the zebrafish result in fin blistering which is due to a disruption of basement membranes [4]. The high phenotypic similarity between *lrp4* morphants and Fraser syndrome gene mutations in zebrafish, therefore, suggests that basement membrane formation and function during fin/limb and kidney development might be regulated by Wnt/β-Catenin and/or Jagged–Notch signaling pathways. Although the expression of Fraser syndrome genes *fras1* and *frem2* were mildly upregulated upon the knockdown of *lrp4* in zebrafish (Fig. 4a), it remains unclear whether there is any direct regulatory relationship between Wnt/Notch signaling and Fraser syndrome gene expressions. Unexpectedly, the swelling and abnormal blood accumulation at the caudal vein plexus was found in *lrp4* morphants (Fig. S4B), suggesting the importance of *lrp4* during blood vessel formation that is difficult to be observed in mammals. It remains to be explored whether the blood vasculature phenotype was due to defective regulation of Wnt/β-catenin or Jagged–Notch signaling.

**Acknowledgements** We are indebted to the family for kindly partaking in this study. We are grateful to Prof. Bernd Wollnik, Dr. Thomas J. Carney and Prof. David Virshup for the kind provision of plasmids. We also thank Prof. Baojie Li for the kind gift of MC3T3-E1 cell line; Prof. Christoph Englert for the kind gift of the *Tg(wt1b:GFP)(line 1)* zebrafish strain; Dr. Xingang Wang and Ms. Pang Zhan for assistance on gene cloning; Mr. Kuan-Chieh Wang for statistical help; Ms. Wei-Ru (Lydia) Hsiao and Chia-Yu Chang for aquarium care; the Taiwan Zebrafish Core Facility at NHRI (TZCF@NHRI), the Taiwan Zebrafish Core Facility at Academia Sinica (TZCAS) and Northwest University Zebrafish Core Facility for assistance with fish culture.

**Authors' contributions** JT and Y-WL conceived the study, designed the experiments and prepared the manuscript. JS, CL, H-YH, C-WC, GL, YK, Y-HC, M-JC, ZL, W-LC, Y-FC and Y-HS prepared the samples, performed the experiments and analyzed the data. MS, ME-K, and OQS diagnosed the patient.

**Funding** This work was supported by Natural Science Foundation of Shaanxi Province, China (2016JM3018); Opening Foundation of State Key Laboratory of Freshwater Ecology and Biotechnology, China (2018FB10); Ministry of Science and Technology, Taiwan (MOST) 106-2313-B-029-002-MY3, 105-2313-B-029-002 and 102-2628-B-029-002-MY3.

## Compliance with ethical standards

**Conflict of interest** The authors declare no competing financial interests.

## References

1. Nakamura T, Gehrke AR, Lemberg J, Zymaszek JS, Shubin NH (2016) Digits and fin rays share common developmental histories. Nature 537:225
2. Grandel H, Schulte-Merker S (1998) The development of the paired fins in the zebrafish (Danio rerio). Mech Dev 79:99–120
3. Tian J, Ling L, Shboul M et al (2010) Loss of CHSY1, a secreted FRINGE enzyme, causes syndromic brachydactyly in humans via increased NOTCH Signaling. Am J Hum Genet 87:768–778
4. Carney TJ, Feitosa NM, Sonntag C et al (2010) Genetic analysis of fin development in zebrafish identifies furin and hemicentin 1 as potential novel fraser syndrome disease genes. PLoS Genet 6:e1000907
5. Lieschke GJ, Currie PD (2007) Animal models of human disease: zebrafish swim into view. Nat Rev Genet 8:353–367
6. Gerlach GF, Wingert RA (2013) Kidney organogenesis in the zebrafish: insights into vertebrate nephrogenesis and regeneration. Wiley Interdiscip Rev Dev Biol 2:559–585
7. Cenani A, Lenz W (1967) Total syndactylia and total radioulnar synostosis in 2 brothers. A contribution on the genetics of syndactylia. Z Kinderheilkd 101:181–190
8. Leupin O, Piters E, Halleux C et al (2011) Bone overgrowth-associated mutations in the LRP4 gene impair sclerostin facilitator function. J Biol Chem 286:19489–19500
9. Ohkawara B, Cabrera-Serrano M, Nakata T et al (2014) LRP4 third beta-propeller domain mutations cause novel congenital myasthenia by compromising agrin-mediated MuSK signaling in a position-specific manner. Hum Mol Genet 23:1856–1868
10. Rivadeneira F, Styrkarsdottir U, Estrada K et al (2009) Twenty bone-mineral-density loci identified by large-scale meta-analysis of genome-wide association studies. Nat Genet 41:1199-U1158
11. Pevzner A, Schoser B, Peters K et al (2012) Anti-LRP4 autoantibodies in AChR- and MuSK-antibody-negative myasthenia gravis. J Neurol 259:427–435
12. Johnson EB, Hammer RE, Herz J (2005) Abnormal development of the apical ectodermal ridge and polysyndactyly in Megf7-deficient mice. Hum Mol Genet 14:3523–3538
13. Simon-Chazottes D, Tutois S, Kuehn M et al (2006) Mutations in the gene encoding the low-density lipoprotein receptor LRP4 cause abnormal limb development in the mouse. Genomics 87:673–677
14. Weatherbee SD, Anderson KV, Niswander LA (2006) LDL-receptor-related protein 4 is crucial for formation of the neuromuscular junction. Development 133:4993–5000
15. Tanahashi H, Tian QB, Hara Y, Sakagami H, Endo S, Suzuki T (2016) Polyhydramnios in Lrp4 knockout mice with bilateral kidney agenesis: defects in the pathways of amniotic fluid clearance. Sci Rep 6:20241
16. Li Y, Pawlik B, Elcioglu N et al (2010) LRP4 mutations alter Wnt/beta-catenin signaling and cause limb and kidney malformations in Cenani-Lenz syndrome. Am J Hum Genet 86:696–706
17. Khan TN, Klar J, Ali Z, Khan F, Baig SM, Dahl N (2013) Cenani-Lenz syndrome restricted to limb and kidney anomalies associated with a novel LRP4 missense mutation. Eur J Med Genet 56:371–374
18. Tamai K, Semenov M, Kato Y et al (2000) LDL-receptor-related proteins in Wnt signal transduction. Nature 407:530–535
19. Pinson KI, Brennan J, Monkley S, Avery BJ, Skarnes WC (2000) An LDL-receptor-related protein mediates Wnt signalling in mice. Nature 407:535–538
20. Kim N, Stiegler AL, Cameron TO et al (2008) Lrp4 is a receptor for Agrin and forms a complex with MuSK. Cell 135:334–342
21. Zhang B, Luo SW, Wang Q, Suzuki T, Xiong WC, Mei L (2008) LRP4 serves as a coreceptor of agrin. Neuron 60:285–297
22. Choi HY, Dieckmann M, Herz J, Niemeier A (2009) Lrp4, a novel receptor for Dickkopf 1 and Sclerostin, Is expressed by osteoblasts and regulates bone growth and turnover In vivo. PLoS One 4:e7930
23. Ahn Y, Sims C, Logue JM, Weatherbee SD, Krumlauf R (2013) Lrp4 and Wise interplay controls the formation and patterning of

mammary and other skin appendage placodes by modulating Wnt signaling. Development 140:583–593
24. Karner CM, Dietrich MF, Johnson EB et al (2010) Lrp4 regulates initiation of ureteric budding and is crucial for kidney formation—a mouse model for Cenani-Lenz syndrome. PLoS One 5:e10418
25. Choi HY, Liu Y, Tennert C et al (2013) APP interacts with LRP4 and agrin to coordinate the development of the neuromuscular junction in mice. Elife 2:e00220
26. Ohazama A, Johnson EB, Ota MS et al (2008) Lrp4 modulates extracellular integration of cell signaling pathways in development. PLoS One 3:e4092
27. Ahn Y, Sims C, Murray MJ et al (2017) Multiple modes of Lrp4 function in modulation of Wnt/beta-catenin signaling during tooth development. Development 144:2824–2836
28. Lu Y, Tian QB, Endo S, Suzuki T (2007) A role for LRP4 in neuronal cell viability is related to apoE-binding. Brain Res 1177:19–28
29. Westerfield M (2000) The zebrafish book: guide for the laboratory use of zebrafish (Danio rerio). Univ. of Oregon Press, Eugene
30. Kimmel CB, Ballard WW, Kimmel SR, Ullmann B, Schilling TF (1995) Stages of embryonic development of the zebrafish. Dev Dynam 203:253–310
31. Chou CW, Zhuo YL, Jiang ZY, Liu YW (2014) The hemodynamically-regulated vascular microenvironment promotes migration of the steroidogenic tissue during its interaction with chromaffin cells in the zebrafish embryo. PLoS One 9:e107997
32. Tian J, Yam C, Balasundaram G, Wang H, Gore A, Sampath K (2003) A temperature-sensitive mutation in the nodal-related gene cyclops reveals that the floor plate is induced during gastrulation in zebrafish. Development 130:3331–3342
33. Chou CW, Lin J, Hou HY, Liu YW (2016) Visualizing the interrenal steroidogenic tissue and its vascular microenvironment in zebrafish. J Vis Exp 118:e54820
34. Tucker B, Lardelli M (2007) A rapid apoptosis assay measuring relative acridine orange fluorescence in zebrafish embryos. Zebrafish 4:113–116
35. Louw JJ, Bastos RN, Chen XW et al (2018) Compound heterozygous loss-of-function mutations in KIF20A are associated with a novel lethal congenital cardiomyopathy in two siblings. PLoS Genet 14:e1007138
36. Liu YW, Guo L (2006) Endothelium is required for the promotion of interrenal morphogenetic movement during early zebrafish development. Dev Biol 297:44–58
37. Chou CW, Lin J, Jiang YJ, Liu YW (2017) Aberrant global and Jagged-mediated Notch signaling disrupts segregation between wt1-expressing and steroidogenic tissues in zebrafish. Endocrinology 158:4206–4217
38. Pan YH, Liu ZY, Shen J, Kopan R (2005) Notch 1 and 2 cooperate in limb ectoderm to receive an early Jagged2 signal regulating interdigital apoptosis. Dev Biol 286:472–482
39. Sidow A, Bulotsky MS, Kerrebrock AW et al (1997) Serrate2 is disrupted in the mouse limb-development mutant syndactylism. Nature 389:722–725
40. Hilton MJ, Tu XL, Wu XM et al (2008) Notch signaling maintains bone marrow mesenchymal progenitors by suppressing osteoblast differentiation. Nat Med 14:306–314
41. Kariminejad A, Stollfuss B, Li Y et al (2013) Severe Cenani-Lenz syndrome caused by loss of LRP4 function. Am J Med Genet A 161A:1475–1479
42. Lindy AS, Bupp CP, McGee SJ et al (2014) Truncating mutations in LRP4 lead to a prenatal lethal form of Cenani-Lenz syndrome. Am J Med Genet A 164:2391–2397
43. Watanabe N, Tezuka Y, Matsuno K et al (2003) Suppression of differentiation and proliferation of early chondrogenic cells by Notch. J Bone Miner Metab 21:344–352
44. Tao JN, Chen S, Yang T et al (2010) Osteosclerosis Owing to Notch Gain of Function Is Solely Rbpj-Dependent. J Bone Miner Res 25:2175–2183
45. Simpson MA, Irving MD, Asilmaz E et al (2011) Mutations in NOTCH2 cause Hajdu-Cheney syndrome, a disorder of severe and progressive bone loss. Nat Genet 43:303–305
46. Kung AWC, Xiao SM, Cherny S et al (2010) Association of JAG1 with bone mineral density and osteoporotic fractures: a genome-wide association study and follow-up replication studies. Am J Hum Genet 86:229–239
47. Murea M, Park JK, Sharma S et al (2010) Expression of Notch pathway proteins correlates with albuminuria, glomerulosclerosis, and renal function. Kidney Int 78:514–522
48. Niranjan T, Bielesz B, Gruenwald A et al (2008) The Notch pathway in podocytes plays a role in the development of glomerular disease. Nat Med 14:290–298
49. Ma M, Jiang Y-J (2007) Jagged2a-notch signaling mediates cell fate choice in the zebrafish pronephric duct. PLoS Genet 3:e18
50. Liu Y, Pathak N, Kramer-Zucker A, Drummond IA (2007) Notch signaling controls the differentiation of transporting epithelia and multiciliated cells in the zebrafish pronephros. Development 134:1111–1122
51. McGregor L, Makela V, Darling SM et al (2003) Fraser syndrome and mouse blebbed phenotype caused by mutations in FRAS1/Fras1 encoding a putative extracellular matrix protein. Nat Genet 34:203–208
52. Slavotinek AM, Tifft CJ (2002) Fraser syndrome and cryptophthalmos: review of the diagnostic criteria and evidence for phenotypic modules in complex malformation syndromes. J Med Genet 39:623–633